IJCRT.ORG ISSN : 2320-2882

INTERNATIONAL JOURNAL OF CREATIVE RESEARCH THOUGHTS (IJCRT)

An International Open Access, Peer-reviewed, Refereed Journal

Evaluation Of Structural, Optical And Electrical Properties Of Tungsten Doped Nanorods

P.Valli Rani [a], G.Prasad[b]

[a]Department of Physics, Ramachandra College of Engineering, Eluru -534006, Andhrapradesh, India.
[b] Department of Physics, Sasi.Institute of Technology &Engineering, Tadepalligudem -534101, Andhrapradesh, India.

Abstract

A tungsten-doped V_2O_5 ($W_xV_2O_5$; x=6, 10 and 15%) nanorods were synthesized by the wet chemical method followed by annealing at 70ºC for 12 h and 700ºC for 1 h. The influence of dopant concentration on structural, morphological, optical and electrical properties of V_2O_5 nanorods were investigated through SEM-EDS, PL and DC conductivity studies. the anorthic is phase disappeared and emerged as an orthorhombic phase. Also, structural analysis shows that the $W_xV_2O_5$ (x=15%) lattice is found to be secondary phase. The gradual morphological transformation of nanostructures due to the incorporation of tungsten is depicted through SEM/EDS characterizations. The relative differential structure of tungsten-doped V_2O_5 nanorods is promptly registered by SEM analysis. EDS result confirms the presence of tungsten and also oxygen vacancies in doped V_2O_5. Doping induced PL quenching has been observed due to the absorption of energy from the defect emission in the V^{5+} lattice by W^{6+} ions. DC conductivity of $W_xV_2O_5$ with respect to different temperatures is explained by the presence of defects. Further, the colloidal form of pure and n-$W_xV_2O_5$ is used to deposit on p-Si substrate for formation of p-n junction by the nebulizer spray technique and the properties of fabricated diodes are investigated under dark and illumination conditions. Also, the Norde's method is used to evaluate the series resistance and barrier height of the Schottky contact. Further, the transient photocurrent measurements were carried out to analyze the photoresponse of the developed diodes.

Keywords: SEM/EDS; Junction diodes; Electrical properties ; Chemical synthesis

1. Introduction

Semiconducting metal oxide nanomaterials are believed as one of the most pivotal classes of multifunctional materials suitable because of their exceptional physical and chemical properties [1-2]. Due to control in intemperance of the shape and particle size recommends new application possibilities facilitating next generation materials with beloved features. During the last few decades, research on synthesized metal oxide nanoparticles had attracted a considerable interest due to their excellent

electronic, optical and magnetic properties in the quantum confinement system [3]. The confinement of the electrons and the holes within the nanostructures lead to alter in their chemical and physical properties as evaluated from the bulk solids. Because of unique conductance properties, vanadium pentoxide (V_2O_5) has been attracted as an interesting n-type semiconductor with a direct band gap of 2.47 eV [4]. It crystallizes with an orthorhombic unit cell structure belonging to the P_{mnm} space group. Generally, the vanadium oxides are exist in larger variety of oxidation states such as VO (V^{2+}, rocksalt structure), V_2O_3 (V^{3+}, corundum), VO_2 (V^{4+}, rutile), V_2O_5 (V^{5+}, layered orthorhombic) and depending on the atmospheric condition and temperature, the phase changes between their oxides can occur. Amongst all the oxide phase described from the application point of view, a single phase V_2O_5 has concerned more attention due to its most stable form with highest oxidation state which serves as a useful amphoteric oxide and oxidizing agent. Therefore, material properties of V_2O_5 is most probably studied and their potential applications are used in industries as heterogeneous catalysis [5], cathodes for Li^+ batteries [6], electrical and optical switching devices [7] and solar cells [8] etc. A multiplicity of methodologies are used to develop nanostructures of V_2O_5 from V^{5+} precursors including reverse-micelles synthesis [9], sol-gel [10], chemical vapor deposition [11] and pulsed laser deposition [12] among others. Many of the exceeding mentioned methods consists multistep based approaches, which require high temperatures for the synthesis of the desired nanostructures. The wet chemical method is selected owing to the low temperature processing and a high degree of solubility which could be achieved. Besides, the transition metals doping have been widely studied to reduce the band gap of V_2O_5. Currently, a few reports have been carefully listed the efforts to adjust the properties of V_2O_5 by doping with metal ions like Ni [13], Co [14], Ti [15], Zn [16], Cr [17], Cu [18] and Ag [19] and so on. Among, the transition metal elements W^{6+} ions can be considerably decrease the recombination process between dopant cation and V_2O_5 matrix. This transition metal has been efficient in shifting the absorption edge of V_2O_5 to visible light. It is recognized that the tungsten a donor in V_2O_5, which can reduce the hole concentration and show the ways to enhance the electrical resistivity of V_2O_5. Recently, Ji Qi et al. [20] studied the tungsten-doped VO_2 nanoparticles by sol-gel method through hydrothermal synthesis and its response study of dopant concentration and phase transition temperature was reported. In this work deals with the structural, morphological, optical and electrical properties of synthesized nanomaterials were also studied in every aspect to exemplify the importance of W^{6+} substitution in V_2O_5. As an innovative efforts to colloidal form of pure and n-$W_xV_2O_5$ is deposit on p-Si substrate for formation of p-n junction through the nebulizer spray technique and their diode characteristics are investigated by voltage-current measurements.

2. Experimental procedures

2.1. Synthesis of undoped and tungsten-doped V_2O_5 nanoparticles

The pure and tungsten-doped V_2O_5 ($W_xV_2O_5$; where x=5, 10 and 15%) nanoparticles with different dopant concentration were synthesized by the wet chemical route. As a starting and dopant source of the materials such as ammonium metavanadate (NH_4VO_3), H_2O_2, PVP-k30 and sodium tungstenate (Na_2OW) were used analytical-grade without any further purification. The typical synthesis method consists of two steps. In the first step, the required amount of ammonia metavanadate was dissolved in deionized water and an estimated amount of H_2O_2 was added drop by drop to the aqueous ammonium metavanadate solution under stirred condition at room temperature for 30 min to obtain a homogenous solution. Later, the solution became colorless or pale yellow. Then, a certain amount of HNO_3 was added to above the solution and the correct pH value 2 is adjusted [21]. Herein, the addition of HNO_3 into the reaction system until the color turned from pale yellow to dark orange shade. Similarly, a required amount of 0.05 g of PVP was added as a surfactant beyond solution with vigorously stirred for 24 h. After completion of these reaction hours, the solution was allowed to settled yellow yields. Then, the obtained solid yields were filtered, washed with distilled water and absolute alcohol by centrifugation (9000 rpm/15min) for several times and then dried in vacuum oven at 60˚C for 12 h. Finally, the dried powder sample was calcined at 600ºC for 1 h with a heating rate of about 10ºC/min in a muffle furnace and the system was cooled to room temperature with a cooling rate of 5ºC/min, to obtain yellow colored V_2O_5 nanoparticles. For synthesis of tungsten doped V_2O_5 ($W_xV_2O_5$; where x=5, 10 and 15%) nanoparticles, an estimated amount of sodium tungstenate (x) were mixed with aqueous ammonium metavanadate solution. Then, a required amount of H_2O_2 was added drop-wise to the homogenous mixture to get a dark orange shade. Besides, a similar procedure adopted for preparation of pure V_2O_5 was followed by doped samples.

3. Results and discussion

3.1. Structural analysis of pure and W_xVO_2 samples annealed at 70ºC for 12 h

The structure and crystal orientation of pure and tungsten-doped VO_2 (W_xVO_2) samples with nominal composition (x=5, 10 and 15%) are shown in Fig. 1(a). The diffraction pattern consists of intense peak at 2θ values of 14.38º, 18.22º, 20.927, 23.97º and 29.79º corresponding to the diffracting planes (110), (111), (200), (002) and (220) respectively. All the diffraction peaks can be well indexed to the tetragonal phase of VO_2 (JCPDS No: 82-1074). It can be observed that undoped and tungsten-doped samples maintained the same crystal phase. No additional diffraction peaks corresponding to the metallic tungsten, oxides of tungsten or secondary phases are detected for tungsten doped samples. Further from Fig. 1(b), it can be seen that increasing the doping concentration of tungsten ions, the most intense peaks at (110), (111), (200), (002) and (112) shifts to higher angle (2θ) indicating that successful incorporation of tungsten in VO_2 lattice. This shift is attributed to the substitution of smaller ionic radius of W^{6+} (rW^{6+}=0.60 Å) ions to V^{2+} (rV^{2+}=0.93 Å) ions having the larger ionic radius. The lattice parameters for

tetragonal crystal structure of pure and tungsten-doped VO_2 samples were estimated from the equation (1),

$$\frac{1}{d^2} = \frac{h^2 + k^2}{a^2} + \frac{l^2}{c^2} \text{--------(1)}$$

where d-is the lattice spacing of crystallographic plane and hkl are the Miller indices of the reflection plane. The lattice constant 'c' has been calculated from the (002) diffraction peak and its values are presented in Table 1. It is observed that the doping concentration increases the values of lattice parameter 'c' decreases compared to undoped VO_2 and also has been found to be well matched with the standard data, JCPDS card No: 82-1074. Also, the shifting of XRD patterns and corresponding decrease of lattice parameter suggests that tungsten ions are effectively incorporated into the VO_2 lattice. The average crystallite size of the studied samples have been estimated with the help of Debye Scherer's equation (2),

$$D = \frac{k\lambda}{\beta \cos\theta} \text{----------(2)}$$

The optimized crystallite size of pure VO_2 is 25.79 nm, and it was found to be decreased with W^{6+} concentrations (Table 1). From XRD results it is interesting to notice that the synthesized pure and tungsten-doped samples annealed at 60°C for 12 h exhibits the tetragonal phase and the respective phase is transformed to orthorhombic when annealed at 700°C for 1 h which is comparable with earlier report [22].

3.2. Structural analysis of pure and tungsten-doped V_2O_5 samples annealed at 700°C

The phase change and crystal orientation of pure and $W_xV_2O_5$ samples with different dopant concentration are shown in Fig. 1(c). The diffraction peaks at 2θ values of 16.47°, 22.39°, 25.27° and 32.14° corresponds to (200), (001), (110) and (400) crystal planes, which are coincide well with the standard data of pure V_2O_5 orthorhombic phase with a space group P_{mmn} (JCPDS card No: 41-1426). In the figure, the structural analysis of tungsten-doped V_2O_5 were reflects segregation of the secondary phase for dopant concentration at x=15%. Their additional peaks at 2θ of 12.428° and 29.02° (marked by star *) are associated with WV_2O_7 (JCPDS card No: 74-1280). Further, the sharp and highly intense peak of pure and tungsten-doped samples clearly reflects that well crystalline nature of the synthesized materials. Also, the maximum intense peak at 2θ=20.635° corresponds to (001) plane and exhibit the preferred c-axis growth orientation. From Fig. 1(d), it is noticed that major diffraction peaks shift towards lower angle (2θ) at higher level of doping of tungsten. This peaks shifting may be attributed to the ionic radii of the dopant W^{6+} (rW^{6+}=0.60 Å) which is larger than that of ionic radius of V^{5+} ions (rV^{5+}=0.54 Å). The crystallite sizes of pure and doped samples are calculated and listed in Table 2. It is observed that crystallite size of V_2O_5 as 25.26 nm and it is found to decrease with increased concentration of tungsten. The reduction in the crystallite size is due to the distortion in the host V_2O_5 lattice by the W^{6+} ions incorporation which decreased the number of nucleation sites and the subsequent growth rate of V_2O_5.

The structural parameters of dislocation density (δ) and microstrain (ε) were resolved using the relation (3 and 4),

$$\delta = \frac{1}{D^2} \text{--------} (3)$$

$$\varepsilon = \frac{\beta \cos\theta}{4} \text{--------} (4)$$

The estimated values of dislocation density and microstrain are listed in Table 2 and it is clearly showed that the dislocation density of the samples changed by increasing the doping level. The estimated positive values of microstrain for all samples (Table 2), indicates the presence of tensile stress on the samples surface. It seems that the introduction of tungsten atoms into V^{5+} matrix inhibits the crystallite growth and induces the tensile strain. The lattice parameters for orthorhombic pure and doped V_2O_5 samples were calculated from the equation (5),

$$\frac{1}{d_{hkl}} = \sqrt{\frac{h^2}{a^2} + \frac{k^2}{b^2} + \frac{l^2}{c^2}} \text{----------} (5)$$

The calculated lattice parameters are listed in Table 2 and it is noted that the lattice parameters decreases with increasing the doping level. This may be due to the smaller ionic radius of tungsten and the tungsten doped in V^{5+} lattice degrades the crystallinity of the nanoparticles. The volume of unit cell of orthorhombic crystal system can be estimated from the equation (6):

$$V = a*b*c \text{--------} (6)$$

From the Table 2, the volume of 5% tungsten-doped V_2O_5 increases with decrease of microstrain compare to pure V_2O_5 sample. However, the impurity ions shifted to the equilibrium position and forms secondary phases by increasing doping level [23]. Besides, the unit cell volume seems to decrease when increase of dopant concentration 10 to 15%, which may be due to the mismatch between W^{6+} and V^{5+} radii.

3.3. SEM-EDS analysis

Surface morphological exploration of pure and tungsten-doped VO_2 samples with different dopant concentrations are shown in Fig. 2(a-d). It is observed that surface of pure VO_2 sample exhibits irregular micro-rods structure and the average diameter of 1μm and length of 2-3 μm. The morphological change in higher level doping samples clearly observed from the Fig. 2(b-d) and it is found that due to interaction between the micro level particles agglomeration is unavoidable. In this regard, SEM images of pure and tungsten-doped V_2O_5 samples annealed at 600°C for 1 h as shown in Fig. 2(e-h). It can be observed that the surface morphology and particle sizes were different with respect to post-annealing and doping concentrations. By comparing Fig. 2(a-d) with Fig. 2(e-h), it is found that pure and doped samples

annealed at 60°C for 12 h exhibits the micro-rod like particles and annealed at 600°C the microrods were completely transformed to nanorods due to phase transformation. This suggests that surface diffusion phenomenon plays an important role in the growth process of nanorods. It is also note that pure V_2O_5 nanoparticles (Fig. 2(e)), a few agglomerations and clusters of various rod shapes are observed. Upon doping ions into V_2O_5, there was a gradual decrease in grain size. This may be addition of W^{6+} ions into V^{5+} solution increased the number of nucleation sites on the samples, thus resulting in a greater degree of preferential alignment exhibited by smaller grains subsequently giving rise to more dense nanorods. As the doping concentration increases upto 15%, the shape of the particles is significantly altered to the pencil tip end like nanorods. Further, the compositions of the samples were quantitatively characterized by EDS analysis measurement. The EDS spectra of pure and doped samples annealed at 600°C are shown in Fig. 3(a-d). These spectra indicate the presence of V and O as the main components and low concentration levels of W^{6+} ions along with elemental mapping. From Fig. 3(b-d), it is observed an increase in the relative intensities of the tungsten peaks with increasing concentration is also observed which confirms the progressive incorporation of tungsten. This guarantees the uniform distribution of the doped W^{6+} ions as expected in the chemical synthesis process employed in this work. EDS analysis demonstrates that V, O, and W elements are present in the samples and well agreement with the results obtained by XRD analysis.

4. Electrical properties

4.1. DC conductivity (σ) and resistivity (ρ)

In order to measure the electrical conductivity, the synthesized samples were compressed into pellet of 1 cm diameter and 2 mm thickness using hydraulic press under a pressure 7 tones/sq.cm. DC conductivity of the samples was measured using Keithley 6517 B electrometer by placing pellets between two copper electrodes inside a specially designed conductivity cell. The equivalent circuit diagram used for this measurement was inferred from studies carried out by Saraswat et al [25]. The current-voltage (I-V) characteristics with sweep voltage ranging from 1-10 V are shown in Fig. 6(a-d) and it is found that the samples exhibit good ohmic behavior. Fig. 7(a-d) represents the variation of room temperature (R_T) electrical resistivity vs. conductivity of different tungsten dopant concentration. It is observed that conductivity increases upto 5% tungsten-doping compared to undoped V_2O_5 and it is gradually decreased thereafter. In general, the electrical conductivity/resistivity of materials depends upon defects, chemical composition, crystalline size, scattering of 'charge carriers' etc. Therefore, the author suggests that tungsten in V^{5+} matrix acts as a deep donor and decreases the concentration of intrinsic donors as a resulting in the decrease of electrical conductivity. Fig. 7(a-d) presents the decrease in resistivity with an increase in temperature is because of the increase in drift mobility of charge carriers and increase in temperature help the bound charges to be freed and participate in the conduction process resulting thereby decrease of resistivity. The negative temperature co-efficient of conductance is observed for all the compositions of tungsten indicates the semiconducting behavior of the studied samples. In general, the characteristics of semiconductor with increasing temperature leads to an increase in the number of

electron-hole pairs resulting in an increased conductivity and it is the characteristics of "thermal activated behavior". The temperature-dependence of DC conductivity satisfies the Arrhenius equation (7),

$$\sigma_{dc} = \sigma_o \exp^{[-E_a/K_BT]} \text{----------(7)}$$

The Arrhenius plots of ln (σ_{dc}) vs. 1000/T for studied samples are shown in Fig. 7(e). This plot indicates an increase in conductivity with temperature that may be due to a hopping mechanism between coordinating sides, local structural relaxations and segmental motions of the samples. It is clear that two linear regions with different slopes were distinguished one at relatively high-temperature and another at low-temperature. This behavior is due to the conduction phenomena of the V^{5+} proceeds through two distinct conduction mechanisms. The conduction mechanism at the higher temperature range is because of the carrier excitation into the extended states beyond the mobility edge and at the lower temperature is due to carrier excitation into localized state at the edge of the band. The two-stage temperature dependence of conductance (σ) is represented by the equation (8),

$$\sigma = \sigma_L \exp\left(\frac{E_{aL}}{K_BT}\right) + \sigma_H \exp\left(\frac{E_{aH}}{K_BT}\right) \text{----------(8)}$$

The estimated values of E_{aH} and E_{aL} are reported in the Table 3. The increase of the activation energy with the W^{6+} doping concentration is resultant impact of coulomb attraction between the electron and the ionized impurities.

4.2. Current-voltage characteristics of Ag/$W_xV_2O_5$/p-Si/Ag diodes

Fig. 8(a-d) shows the current-voltage characteristics of undoped and tungsten-doped (5%, 10% and 15%) V_2O_5/p-Si diodes were measured at room temperature. All the curves were asymmetrical and non-linear. The current density-voltage (J-V) characteristics of the pure and tungsten-doped V_2O_5/p-Si diodes under dark condition are shown in Fig. 8(e).These diodes exhibit rectification like behavior. The rectification ratio (RR) is estimated as the ratio of forward current density (J_F) to the reverse current density (J_R) at a certain applied voltage (V), i.e., $RR=(J_F/J_R)^V$. The RR is found to be dependent on the substitution of tungsten content and its values are given in Table 3. It is observed that RR decreases with increasing the dopant concentration. This may be the grain boundary scattering and limited mobility of charge carriers plays an important role in the decrease of RR values. This deprived transport properties could not provide effective direct electrical pathway for the electrons. The impact in the rectification ratio due to the applied bias reveals that the current in the diodes is controlled by space charge limited theory [27]. According to the space charge theory, the unbalanced charge can be easily produced by the applied voltage and also signify the trap induced current flow, in which, the traps capture the injected charges thereby reducing the rectification ratio. With the increase in applied bias voltage, the corresponding injection rate increases the filling of trap levels. Therefore, the current will increase quickly and the rectification rate will also increase the trap free zone. The thermionic emission current-voltage dependence of the junction of the applied voltage (V) may be written as the equation (9) [28],

$$I = I_s\left[\exp\left(\frac{qV}{nKT}\right)-1\right]\left(V \geq 3k_B\, T/q\right)----------(9)$$

The saturation current I_s-is expressed by the equation (10),

$$I_s = AA^*T^2\exp\left(-\frac{q\Phi_B}{KT}\right)----------(10)$$

The ideality factor, n-can be calculated from the straight line region of the slope during forward bias ln (I)-V plot and can be written by the equation (11),

$$n = \frac{q}{KT}\frac{dV}{d(\ln I)}----------(11)$$

where I_o can be determined by and extrapolation of the forward bias ln (I)-V curve to V=0. The Φ_B is calculated by the following relation (12),

$$\Phi_B = \frac{KT}{q}\ln\left(\frac{AA^*T^2}{I_o}\right)----------(12)$$

The experimental values of Schottky barrier height (Φ_B) and ideality factor (n) were determined from the current axis intercept and the slope of the liner region of the forward bias semi log J-V curve, respectively. The calculated values of n and Φ_B for undoped and tungsten- doped V_2O_5/p-Si diodes are listed in Table 3. It is clearly observed that the tungsten doped V_2O_5/p-Si diodes have lower ideality factor and higher barrier height values compared with undoped V_2O_5/p-Si. The obtained n values confirm the presence resultant currents are due to recombination and diffusion process in these diodes and the decrease in ideality factor may be attributed to the improved interface state of doped diodes. However, the tungsten ion substitution of V_2O_5 lattice reduces the number of oxygen vacancies and leads to lower density of free carriers, which can effectively increase the barrier height at the interface. In order to determine a series resistance and barrier height of the studied diodes, we used Norde method given as the relation (13),

$$F(V) = \frac{V_o}{\gamma} - \frac{kT}{q}\left(\frac{I(V)}{A^*AT^2}\right)----------(13)$$

Fig. 8(f) shows the plots of F(V) vs. voltage for the diodes and the plots give a minimum point and thus, from these plots, the barrier height value for the diodes can be determined using the equation (14).

$$\phi_B = F\left(V_o\right) + \frac{V_o}{\gamma} - \frac{kT}{q}----------(14)$$

where $F(V_o)$ is the minimum point of F(V) function and V_o is the corresponding voltage. According to the F(V)-V curves, the effective Schottky barrier height for undoped V_2O_5 structure is estimated to be 0.423 eV while for $W_xV_2O_5$/p-Si is 0.442-0.448 eV. There is a good agreement between the values of Φ_B obtained from the Norde functions from I-V measurements (Table 3). It is observed that the barrier height increase with increasing tungsten-doping concentration, because the tungsten-substitution changes the position of Fermi level in V_2O_5. Also, in Norde method, the series resistance is determined as the following relation (15),

$$R_s = \frac{kT(\gamma - n)}{qI_o} \text{----------(15)}$$

The R_s values according to the Norde method are listed in Table 3. It is seen that the series resistance increases with increasing tungsten-substitution due to the surface morphology and electrical properties of the samples. In Addition, the current density-voltage (J-V) characteristics of studied diodes under an illumination are shown in Fig. 9(a). It can be observed that all diodes always reveal good rectifying behavior. It is mainly due to the generated electron-hole pairs, i.e., neutral excitons and these charges contribute to the photocurrent as a result of the light absorption. It indicates that the rectification effect is weakened and the diodes exhibit more ideal behavior under illumination. The potential parameters such as open circuit voltage (V_{oc}), short-circuit current (J_{sc}), current density (J_m) and maximum power point (V_m) are established through Fig. 9(a). The filling factor (FF) and conversion efficiency (η) can be estimated as the solar cell parameters [29] and it values are present in Table 3. It is observed that the device have a low conversion efficiency and low fill factor which are ascribed to series resistance or recombination current in the space charge region of the device. The photoresponse of the device was investigated with the help of transient photocurrent measurements. The time-dependent photocurrent of this device is measured at 4 V under a 375 nm light under "ON" and "OFF" condition (Fig. 9(b)). The response and decay time were about 3 s and 20 s, respectively. In every case it is witnessed that in the turning ON state, the current of the diode rapidly increased to a certain level and then gradually tends to the maximum value. After turn OFF, the current came back to its initial state. The ratio of current $I_{ON/OFF}$ for the diode is resulted to be about 30 s. This suggested that the diode exhibits a high $I_{ON/OFF}$ ratio. However, the diode is illuminated, the number of photo-generated charge carries increased and the electrons contributed to the current. Subsequently, turn OFF the light the number of free electrons reduced and the current of the diode decreased. The photo-conducting properties of the diodes are depends on the trap centers present in the pure and tungsten-doped V_2O_5 nanomaterials. This suggests that the fabricated diodes exhibit a photoconducting behavior.

Conclusion

The structural, optical and electrical properties of tungsten doped V_2O_5 nanoparticles with different dopant concentration were studied through the respective instrumentation method and their results are reported along with the suitable illustrations. SEM analysis of pure and tungsten doped samples were annealed at 70^oC exhibits anorthic phase and annealing at 700^oC the anorthic phase disappeared and emerged as orthorhombic phase. The inclusion of tungsten into V_2O_5 crystal structure is promised by XRD patterns and it is exhibit that the average crystal size was found to decrease with the increase in tungsten-concentration. With tungsten incorporation, a gradual morphological transformation of nanostructures is demonstrated vividly through SEM/TEM characterizations. The SAED pattern results showed that all the samples have enhanced crystalline quality with the orthorhombic structure of V_2O_5, even substitution with various tungsten concentration. Doping induced PL quenching has been proposed to be due to the absorption of energy from the defect emission in the V^{5+} lattice by W^{6+} ions. DC electrical conductivity with respect to different temperatures is explained by the presence of defects and it is confirm that studied samples with increasing temperature for thermally activated process. We report on the synthesized pure and tungsten doped V_2O_5 nanopowders to make in colloidal form and are deposit on p-Si substrate for formation of junction diode by the nebulizer spray technique and their device properties of fabricated diodes were investigated under dark and illumination condition. Also, the Norde's method was used to evaluate the I-V characteristics and to obtain the series resistance and barrier height of the Schottky contact.

References

[1] X. Wang, C.J. Summers, Z.L. Wang, Large-Scale Hexagonal-Patterned Growth of Aligned ZnO Nanorods for Nano-optoelectronics and Nanosensor Array, Nano Lett. 4 (2004) 423-426.

[2] J.G. Wang, M.-L. Tian, T.E. Mallouk, M.H.W. Chan, Microstructure and Interdiffusion of Template-Synthesized Au/Sn/Au Junction Nanowires, Nano Lett. 4 (7) (2004) 1313-1318.

[3] M.K. Naskar, A. Patra, M. Chatterjee, Understanding the role of surfactants on the preparation of ZnS nanocrystals, J. Colloid Interface Sci. 297 (2006) 271-275.

[4] N. Van Hieu, D. Lichtman, Bandgap radiation induced photodesorption form V_2O_5 powder and vanadium oxides surfaces, J. Vac. Sci. Technol. 18 (1981) 49-53.

[5] A. Legrouri, T. Baird, J.R. Fryer, Electron Optical Studies of Fresh and Reduced Vanadium Pentoxide-Supported Rhodium Catalysts, J. Catal. 140 (1993) 173-183.

[6] V.M. Mohan, B. Hu, W. Qiu, W. Chen, Synthesis, structural and electrochemical performance of V_2O_5 nanotubes as cathode material for lithium battery, J. Appl. Electrochem. 39 (2009) 2001-2006.

[7] G.T. Kim, J. Muster, V. Krstic, Y.W. Park, S. Roth, and M. Burghard, Field-effect transistor made of individual V_2O_5 nanofibers. Appl. Phys. Lett. 76 (2000) 1875-1877.

[8] J. Wu, Y. Zhang, Y. He, C. Liu, W. Guolt, S. Ruan, Application of solution-processed V_2O_5 in inverted polymer solar cells based on fluorine-doped tin oxide substrate, J. Nanosci Nanotechnol. 14 (2014) 4214-7.

[9] N. Pinna, M. Willinger, K. Weiss, J. Urban, R. Schlogl, Local Structure of Nanoscopic Materials: V_2O_5 Nanorods and Nanowires, Nano. Lett. 3 (2003) 1131-1134.

[10] Z. Wang, J. Chen, X. Hu, Electro-chromic properties of aqueous sol-gel derived vanadium oxide films with different thickness, Thin Solid Films. 375 (2000) 238-241.

[11] Y. Wnang, Q. Su, C.H. Chen, M.L. Yu, G.J. Han, G.Q. Wang, K. Xin, W. Lan and X.Q. Liu, Low temperature growth of vanadium pentoxide nanomaterials by chemical vapour deposition using VO $(acac)_2$ as precursor, J. Phys. D: Appl. Phys. 43 (2010) 183001-185402.

[12] C.V. Ramana, R.J. Smith, O.M. Hussain, C.M. Julien, on the growth mechanism of pulsed-laser deposited vanadium oxide thin films, Mater. Sci. Eng. B. 111 (2004) 218-225.

[13] R. Suresh, K. Giribabu, R. Manigandan, S. Praveen Kumar, S. Munusamy, S. Muthmizh, A. Stephen, V. Narayanan, New electrochemical sensor based on Ni-doped V_2O_5 nanoplates modified glassy carbon electrode for selective determination of dopamine at nanomolar level, Sensors and Actuators B: Chem. 202 (2014) 440-447.

[14] S. Pavasupree, Y. Suzuki, A. Kitiyanan, S.P. Art, S. Yoshikawa, Synthesis and characterization of vanadium oxides nanorods, J. Sol. Stat. Chem, 178 (2005) 2152-2158.

Figure captions

Fig.1. XRD pattern of (a) W_xVO_2 (x=0, 5, 10 and 15%) samples annealed at 60^{o}C for 12 h, (b) a shift position of W_xVO_2, (c) $W_xV_2O_5$ samples annealed at 600^{o}C for 1 h and (c) a shift position of $W_xV_2O_5$.

Fig.2. SEM images of (a-d) pure and W_xVO_2 samples annealed at 60^{o}C for 12 h and (e-h) pure and $W_xV_2O_5$ samples annealed at 600^{o}C for 1 h.

Fig.3. Current-voltage (I-V) characteristics of (a) pure and (b-d) $W_xV_2O_5$ (where x=0, 5, 10, and 15%) samples.

Fig.4. Temperature-dependent DC electrical conductivity vs. resistivity of (a) pure, (b-d) $W_xV_2O_5$ (where x=0, 5, 10, and 15%) samples and (e) activation energy.

Figure 1

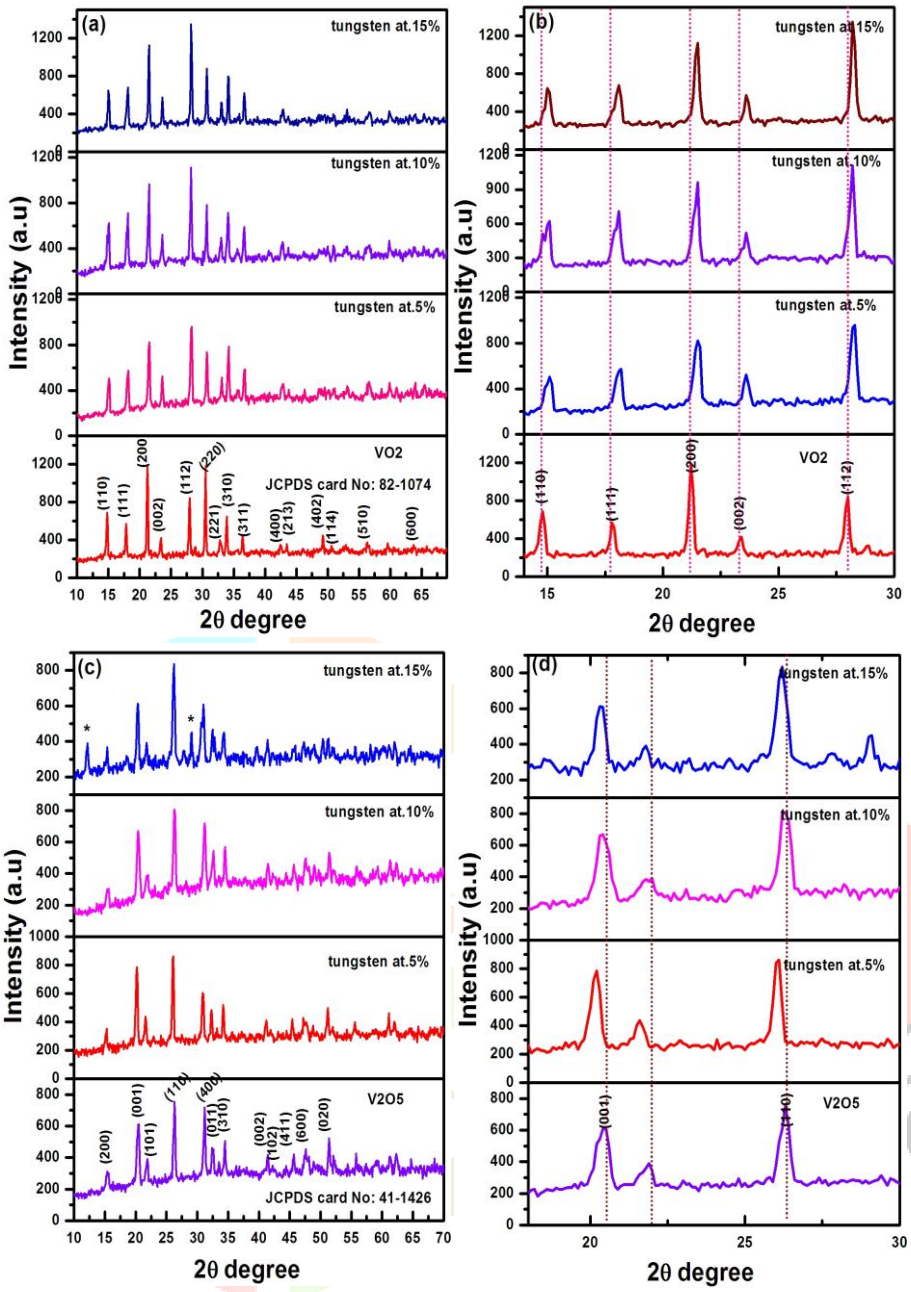
(a)
tungsten at.15%
tungsten at.10%
tungsten at.5%
VO2
JCPDS card No: 82-1074
(110)
(111)
(002)
(200)
(112)
(220)
(221)
(310)
(311)
(400)
(213)
(402)
(114)
(510)
(600)
Intensity (a.u)
2θ degree
(b)
tungsten at.15%
tungsten at.10%
tungsten at.5%
VO2
(110)
(111)
(200)
(002)
(112)
Intensity (a.u)
2θ degree
(c)
tungsten at.15%
tungsten at.10%
tungsten at.5%
V2O5
JCPDS card No: 41-1426
(200)
(001)
(101)
(110)
(400)
(011)
(310)
(002)
(102)
(411)
(600)
(020)
Intensity (a.u)
2θ degree
(d)
tungsten at.15%
tungsten at.10%
tungsten at.5%
V2O5
(001)
(110)
Intensity (a.u)
2θ degree

Figure 2

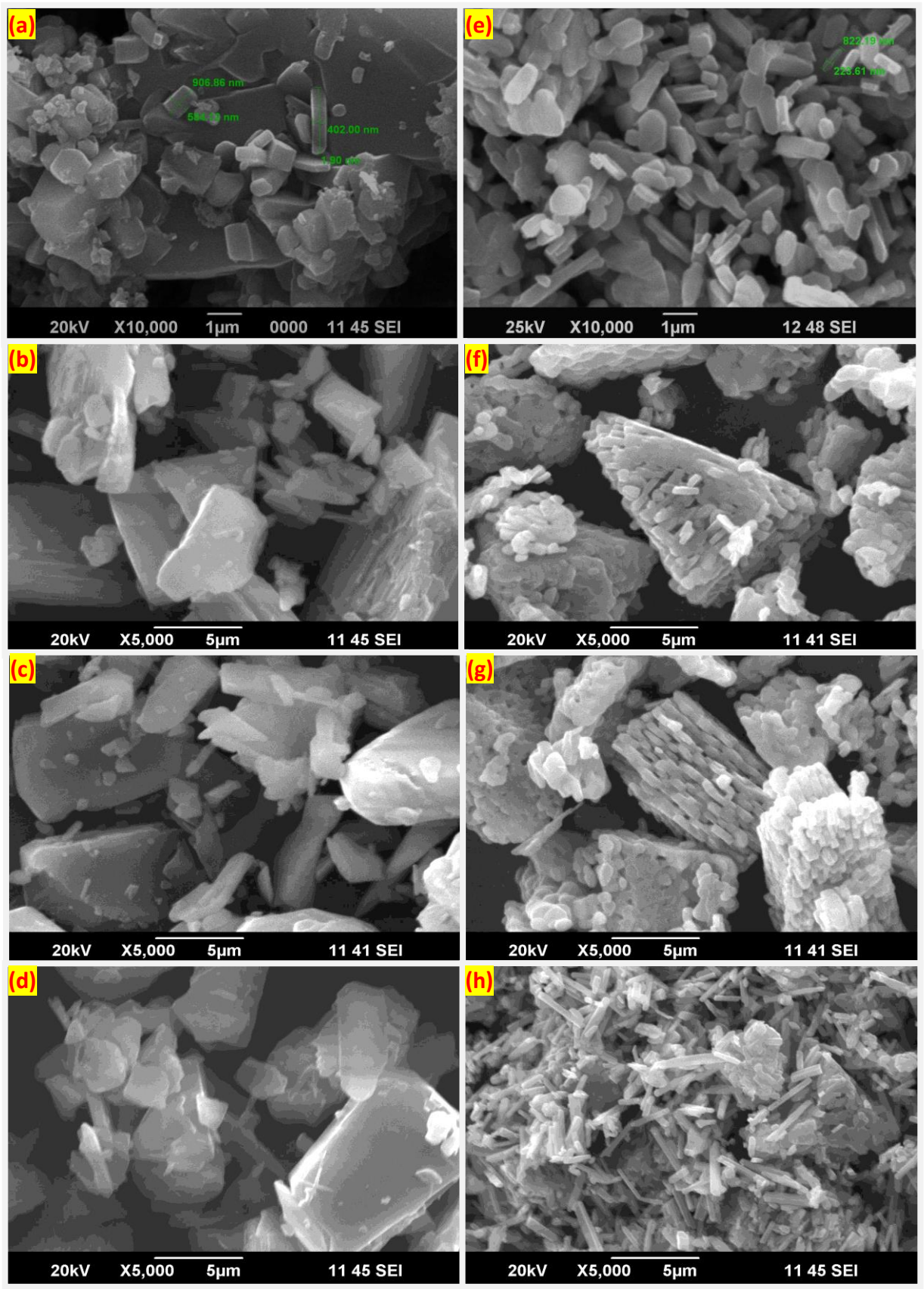
(a)
906.86 nm
584.19 nm
402.00 nm
1.90 nm
20kV X10,000 1µm 0000 11 45 SEI
(e)
822.19 nm
223.61 nm
25kV X10,000 1µm 12 48 SEI
(b)
20kV X5,000 5µm 11 45 SEI
(f)
20kV X5,000 5µm 11 41 SEI
(c)
20kV X5,000 5µm 11 41 SEI
(g)
20kV X5,000 5µm 11 41 SEI
(d)
20kV X5,000 5µm 11 45 SEI
(h)
20kV X5,000 5µm 11 45 SEI

Figure 3

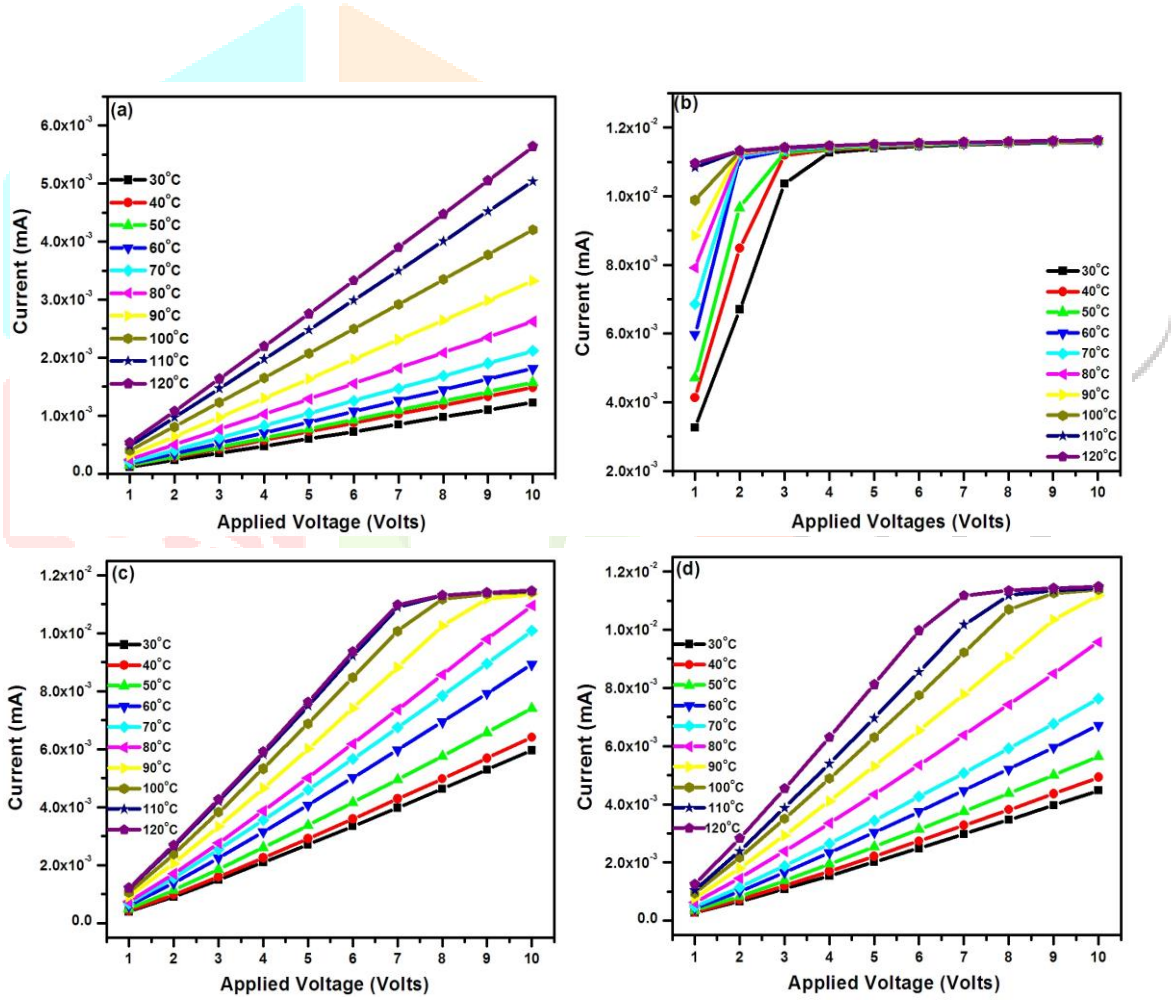
(a)
Current (mA)
Applied Voltage (Volts)
(b)
Current (mA)
Applied Voltages (Volts)
(c)
Current (mA)
Applied Voltage (Volts)
(d)
Current (mA)
Applied Voltage (Volts)
30°C
40°C
50°C
60°C
70°C
80°C
90°C
100°C
110°C
120°C

Figure 4

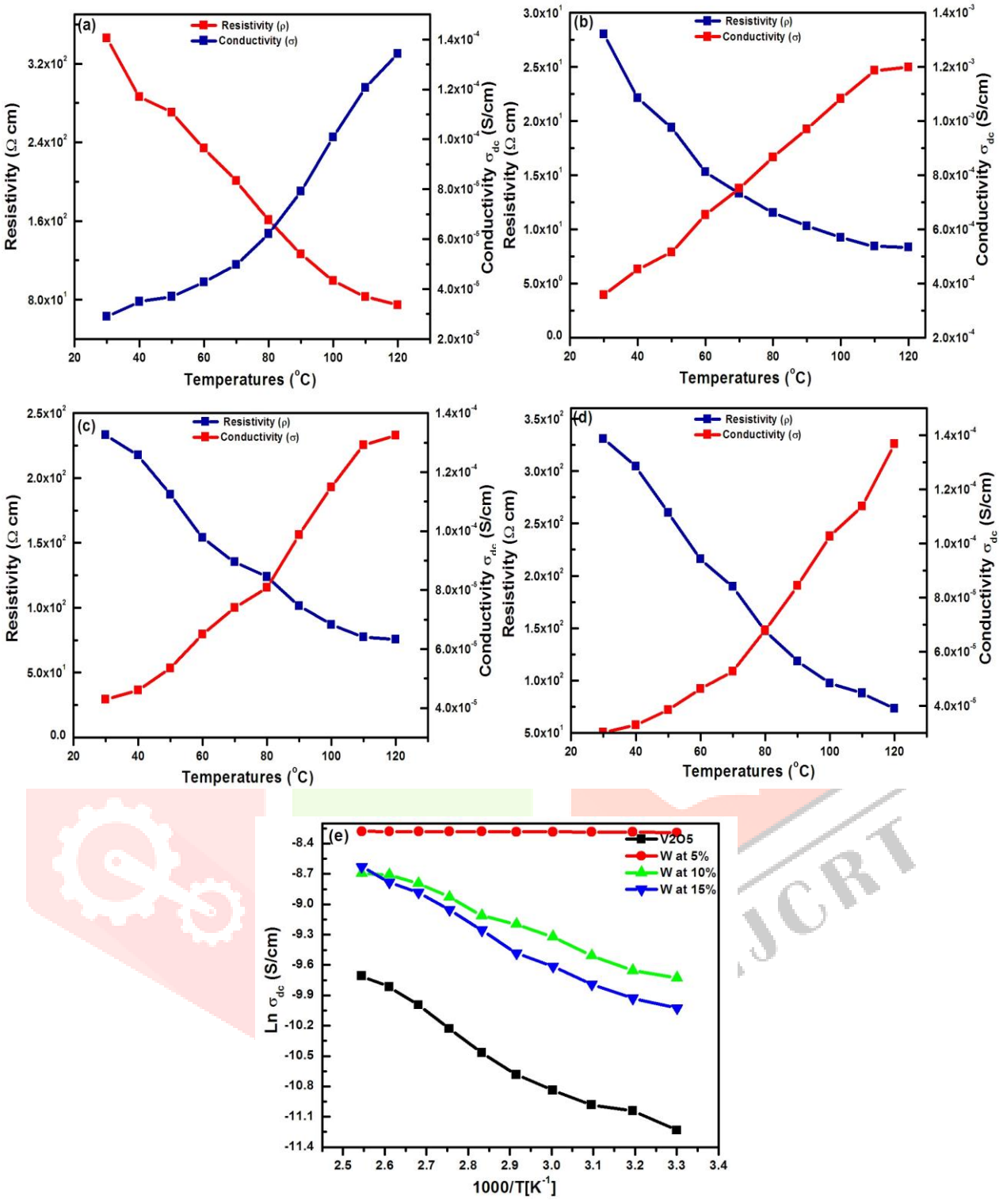
(a)
Resistivity (ρ)
Conductivity (σ)
Resistivity (Ω cm)
Conductivity σdc (S/cm)
Temperatures (°C)
(b)
Resistivity (ρ)
Conductivity (σ)
Resistivity (Ω cm)
Conductivity σdc (S/cm)
Temperatures (°C)
(c)
Resistivity (ρ)
Conductivity (σ)
Resistivity (Ω cm)
Conductivity σdc (S/cm)
Temperatures (°C)
(d)
Resistivity (ρ)
Conductivity (σ)
Resistivity (Ω cm)
Conductivity σdc (S/cm)
Temperatures (°C)
(e)
V2O5
W at 5%
W at 10%
W at 15%
Ln σdc (S/cm)
1000/T[K-1]